Archive of Applied Mechanics manuscript No.
(will be inserted by the editor)

Nicholas Zachariou (for the CLAS Collaboration)

Study of the Few Nucleon Systems at CLAS

Received: date / Accepted: date

Abstract The study of few nucleon systems with electromagnetic probes is an essential component of the scientific program carried out at the Thomas Jefferson Laboratory. Here we present measurements of exclusive reactions on light nuclei using real photon beams with energies up to 3 GeV and the CEBAF Large Acceptance Spectrometer (CLAS), a nearly 4π magnetic spectrometer, in order to study the properties of strongly interacting matter and the transition from hadronic (i.e in terms of nucleons and mesons) to partonic (in terms of quark and gluons) degrees of freedom in nuclear interactions. We discuss the progress made in understanding the relevant degrees of freedom using polarisation observables and unpolarised cross sections of deuteron and ^{3}He photodisintegration in the few-GeV photon-energy region. In addition, recent high-statistics experiments with the CLAS detector have provided us with sufficient counting rates to study the effects of initial- and final-state interactions in reactions off the deuteron. Such data allow us to extract a large set of polarisation observables for final-state interactions in hyperon photoproduction and to study the properties of the hyperon-nucleon interaction. Initial-state effects are studied by mapping the dependence of experimental observables on the spectator-nucleon momentum. We also present recent results for polarisation observables for quasi-free $K^+\Lambda$ off the bound proton in a deuteron as well as for final-state interactions in the reaction $\gamma d \to K^+\Lambda n$, and will discuss their impact on hyperon-nucleon studies.

Keywords Thomas Jefferson Lab · CLAS · Dimensional scaling · Constituent counting rules · Hyperon-nucleon interaction

1 Introduction

The Continuous Electron Beam Accelerator Facility (CEBAF) at JLab provides the multi-GeV continuous wave beams essential for experiments at the nuclear and particle physics interface [1]. The race-track shaped accelerator comprised two linear accelerators linked together (total of 338 accelerating cavities) and was able to accelerate electron beam bunches up to 6 GeV by recirculating the beam up to five times[1] (see Fig. 1). The accelerator was operating at 200 μA maximum current with an energy precision of $\Delta E/E \approx 10^{-4}$ and the capability of simultaneously delivering beams of different energies and currents to three experimental end stations. Furthermore, the injector was able to produce polarised beams with polarisation $> 80\%$ – allowing polarisation experiments to be performed.

N. Zachariou
University of Edinburgh
James Clerk Maxwell Building
Peter Guthrie Tait Road
Edinburgh EH9 3FD
Tel.: +44 (0) 131 651 7854
Fax: +44 (0) 131 650 5902
E-mail: nick.zachariou@ed.ac.uk

[1] The accelerator has now been upgraded and is able to deliver beams with energies up to 12 GeV

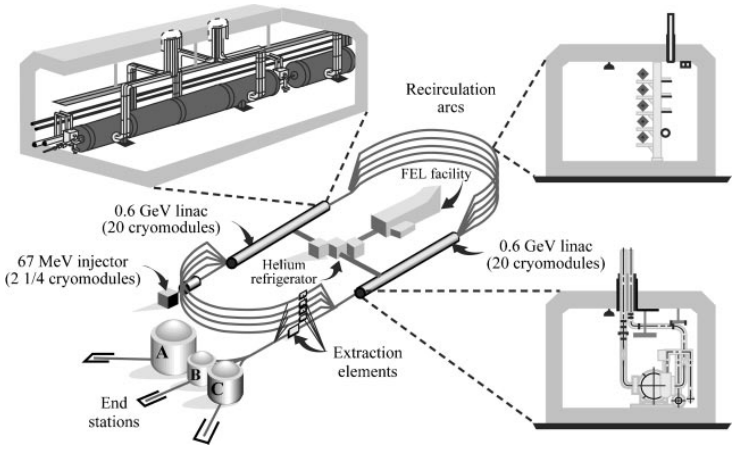

Fig. 1 Schematic CEBAF accelerator overview.

The three end stations (Halls A, B, and C) were focused on performing complementary experiments using two identical High-Resolution Spectrometers (Hall A), a Large Acceptance Spectrometer (Hall B), and High-Momentum and Short-Orbit Spectrometers (Hall C). The CEBAF Large Acceptance Spectrometer (CLAS) [2], which was the main scientific instruments for experiments in Hall B until 2012, provided a nearly hermetic acceptance and was well suited for a broad experimental programme to study the structure and interactions of mesons, nucleons, and nuclei using polarized and unpolarized electron and photon beams and targets.

The CLAS detector was split into six identical mass spectrometers by six kidney-shaped superconducting coils, which produced a toroidal magnetic field primarily in the ϕ direction. Each sector was composed of three layers of drift chambers to measure charged particle trajectories, scintillators to measure time-of-flight, a Cerenkov counter to separate electrons and π^-'s, and electromagnetic calorimeters primarily used for photon and neutron identification (see left panel in Fig. 2). These components allowed charged particle tracking between 8° and 144° and neutral particle detection between 8° and 70° with excellent momentum and angular resolutions ($\Delta p/p \sim 0.5\%$, $\sigma_\theta \sim 1$ mrad, $\sigma_\phi \sim 4$ mrad). The detector characteristics allowed precise particle identification between protons and pions below 3.5 GeV/c, and between pions and kaons below 2 GeV/c.

Hall B also housed the tagger spectrometer placed upstream the CLAS detector allowing real-photon experiments to be performed (see right panel of Fig. 2). Photons with energies between 20% and 95% of the incident electron energy E_0 were tagged using a hodoscope to detect the electrons that underwent bremsstrahlung. The segmentation of the two layers of scintillators in the hodoscope

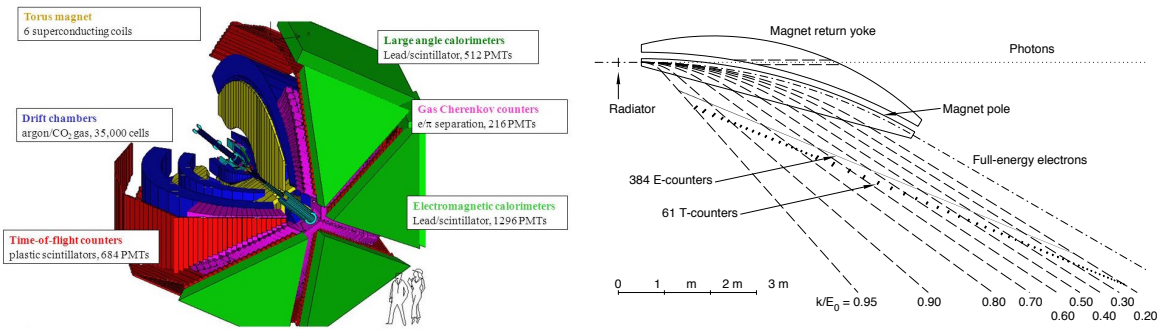

Fig. 2 Left: schematic CLAS detector. The kidney-shaped superconducting coils are shown in yellow, drift chambers in blue, Cerenkov counters in magenta, time-of-flight scintillators in red, and electromagnetic calorimeters in green. Right: Hall B photon tagging system located upstream of the CLAS detector.

(labeled as E-counters and T-counters in Fig. 2) provided an energy resolution of $0.001E_0$, and a timing resolution of 110 ps. The use of amorphous and crystal radiators allowed for circularly and linearly polarized experiments to be performed with average polarisations of 80% and 75% respectively. These capabilities were utilised in a plethora of experiments performed in Hall B and here we report recent measurements on the study of few nucleon systems to obtain detailed understanding of the underlying dynamics in transition region and the hyperon-nucleon interaction.

2 Studies of the Transition Region

Understanding the fundamental properties of the region between the two pictures of nuclear interaction – the hadronic, which describes well the interaction in the confinement or low-energy regime, and the partonic, which is well understood in the asymptotic freedom or high-energy regime – has been a long standing problem in nuclear physics. Experimentally accessible phenomena, such as dimensional scaling and hadron helicity conservation, are typically employed to search and identify the onset of quark-gluon dynamics. Dimensional scaling rules have been first derived in the framework of perturbative QCD (pQCD) and relate the energy dependence, s, at a high-momentum transfer of the invariant cross section to the number of elementary fields, n, that are involved in the interaction, $d\sigma/dt \propto s^{-n+2}$ [3]. The fundamental origin of the scaling in pQCD stems from the scale invariance of the elementary interactions between the hadron constituents reflecting the property of asymptotic freedom of QCD at small distance scales. More recent theoretical efforts, using the correspondence between string theories in Anti-de-Sitter space-time and conformal field theories in physical space time, have also shown that the same scaling can be derived [4]. This was done by using the scale invariance of the interaction between hadron constituents at very large distance scales in the so-called "conformal window" where the effective coupling is large but constant. Therefore, it was shown that dimensional scaling laws probe the limits of two very different dynamical regimes; one at large momentum transfers where the strong coupling is small, and one at very small momentum transfers.

Nuclear photodisintegration allows us to study both of these regimes and here we report recent measurements done using the CLAS detector. The differential cross section of two-body photodisintegration of ^{3}He was determined using data from experiment E93-044 [5]. This reaction is ideal to study dimensional scaling in the large-distance regime as it was shown that resonance mechanisms at low momentum transfers are significantly suppressed and thus the any scaling will be easy to identify in the low-energy data. In this experiment, a circularly polarised photon beam with energies between 0.35 and 1.55 GeV was incident on a 18-cm long cryogenic liquid ^{3}He target. The detection and identification of the two final-state particles in combination with cuts derived from two-body kinematics allowed a clean dataset to be obtained. The results from CLAS were combined with Hall A data at proton $c.m.$ angle 90° and fitted with $d\sigma/dt = As^{-N}$ to establish the onset of scaling (see Fig. 3).The analysis determined a scaling power of $N = 17 \pm 1$, which is well in agreement with the predictions of dimensional scaling [6]. In addition, CLAS data allowed the determination of the invariant cross-section at other proton angles where no other measurement exists. The CLAS data indicate that the onset of scaling is independent of energy and lies between 0.6 and 0.8 GeV for all angles. Furthermore, the momentum transfer ($t = 0.64$ GeV^2) and proton transversed momentum ($p_\perp = 0.95$ GeV/c) values at the region where the scaling is first observed qualitatively support the conformal window hypothesis. Studies of this reaction at higher photon energies will provide further direct evidence whether AdS/CFT is the appropriate framework to understand the scaling observed, where one expects another onset of scaling of the invariant cross-section in the small-distance regime.

Deuteron photodisintegration had been a flagship process for studying the transition region due to the simplicity of the target and there have been many attempts to theoretically describe the differential cross section of this reaction. CLAS data from experiment E93-017 allowed a nearly complete angular distributions of the two-body deuteron photodisintegration differential cross section between photon energies 0.5 and 3.0 GeV. The results from CLAS were combined with all previous data to study in detail the power law dependence of the invariant cross section (see Fig. 4) [7]. The results showed that the expected scaling of s^{-11} is observed above proton transversed momenta of $p_\perp = 1.1$ GeV/c, indicating that the quark-gluon regime is reached above these energies. The available cross-section data were characterised with the same degree of success by several very different theoretical approaches showing that the cross-section alone does not provide the information we need to obtain a comprehensive understanding of the underlying dynamics.

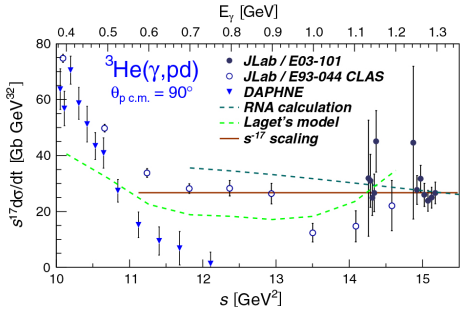

Fig. 3 Recent published results on the invariant cross section of the γ^3He$\rightarrow$ pd reaction at proton $c.m.$ angle 90° scaled by s^{17} to test predictions of dimensional scaling laws [6]. Results from CLAS are shown with open circles and the solid line shows the expected scaling normalised to the highest photon-energy point.

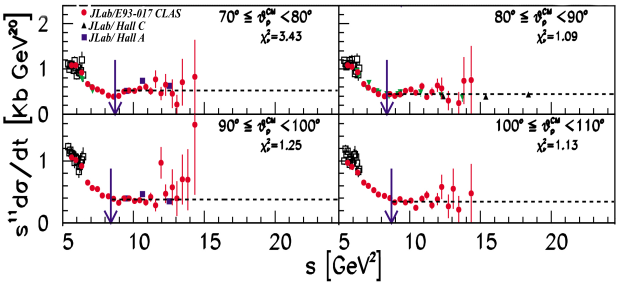

Fig. 4 Published results on the invariant cross section of the $\gamma d \rightarrow pn$ reaction for four angles in the proton $c.m.$ [7]. The cross section data are scaled by s^{11} to test predictions of the dimensional scaling laws. Results from CLAS are shown with the red points. The vertical arrows indicate the s value corresponding to $p_\perp = 1.1$ GeV/c and the dashed lines are fits to the data above $p_\perp = 1.1$ GeV/c.

Polarisation observables, which are easily accessed with CLAS data, provided us with the tools we needed to further constrain available theoretical models that attempt to describe the underlying dynamics of the reaction at these energies. Nonperturbative phenomenological approaches have been typically employed for describing both the scaling behaviour of the cross section as well as polarisation observables. The main models developed for deuteron photodisintegration are the Hard Rescattering Mechanism (HRM) [8], which is described as a phenomenological extension of pQCD, and the Quark-Gluon-String-Model (QGSM) [9], which is a purely non-perturbative partonic model. As mentioned before, both of the models have shown to describe the available cross-section data with the same degree of success [10], however predictions between the models on the beam-spin asymmetry, Σ, which is more sensitive to the reaction mechanism, differ by about 40% [11]. Data from E06-103 [12] experiment performed with the CLAS detector allowed a detail study of the beam-spin asymmetry for a wide range of proton $c.m.$ angles (34° – 145°) and photon energies between 1.1 and 2.3 GeV [13]. Figure 5 shows the available results of the beam-spin asymmetry in the GeV photon-energy region. The energy dependence of the determined Σ shows a clear transition from lower to higher values around 1.7 GeV, that might be described by the HRM model. Neither model predicts, however, the magnitude of the observable. The angular dependence of Σ shows rich structures especially at lower photon energies.

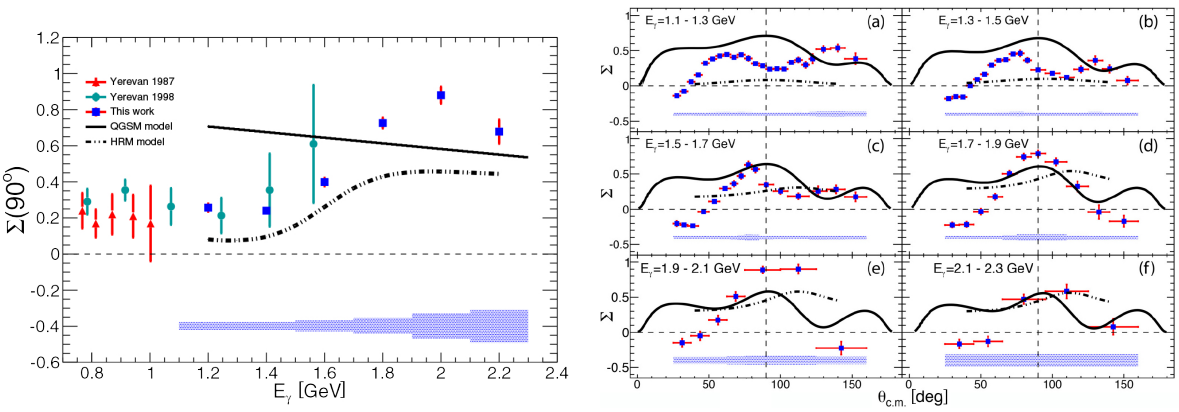

Fig. 5 Recent published data from CLAS on the beam-spin asymmetry of the reaction $\gamma d \rightarrow pn$ [13]. The left panel shows the energy dependence of the 90° data (blue squares) compared to previous measurements from Yerevan. Theoretical predictions from QGSM and HRM are shown with solid and dashed line respectively. The right panel shows the angular dependence for six photon-energy bins 200-MeV wide.

Similar structures are predicted by the QGSM, however, none of the models is able to adequately describe the angular dependence of the CLAS data. Overall, results from CLAS significantly extended the existing database to a much broader kinematic range, improving at the same time the precision of the results. The theoretical description of the data is ongoing and in an attempt to gain insight of the underlying dynamics of nuclear processes in the transition regime. Recent calculations by the HRM model have shown that the model is able to describe well the magnitude and onset of dimensional scaling of the two-body photodisintegration of ^{3}He, giving additional information on the reaction dynamics [14].

3 Studies of the Hyperon-Nucleon Interaction

A comprehensive understanding of the Hyperon-Nucleon (YN) interaction allows us to obtain a detailed picture of the strong interaction, which is currently primarily based on the nucleon-nucleon interaction (NN). The best way to obtain information on the YN interaction is through high-precision hyperon-nucleon scattering experiments. However, due to experimental challenges imposed by the short-lived hyperon beams and targets, performing direct studies of the YN interaction has be a arduous task. Because of this, experimental efforts have been focused on indirect approaches that allow us to infer information on the underlying dynamics. One such approach focuses on studies of hypernuclei – nuclei in which one or more nucleon are replaced by hyperons following a nuclear reaction. Sensitivity to the YN interaction is predicted from the observed hypernuclear energy levels and decays. Although giving valuable input to the YN interaction, such studies have significant model uncertainties related to medium modification and many-body effects. Therefore, alternative and more direct approaches are needed to adequately constrain and understand the YN interaction in detail. Specifically, the study Final-State Interactions (FSI) in exclusive hyperon production reactions provides us with an excellent tool to obtain long-sought information on the YN interaction. Overall, reliable data on the YN interaction will allow for realistic calculations of hypernuclear structure and hyperon matter and will provide essential information needed for addressing the "Hyperon Puzzle", which reflects how theorists cannot reconcile the predicted role of hyperons in neutron stars with the recent observations of large-mass neutron stars [15]. A detailed study and understanding of FSI will also allows us to better understand initial-state effects in bound targets, such as the neutron in deuterium.

CEBAF and Hall-B at JLab allow detailed studies of the YN interaction utilising the high counting rates provided by the modern accelerator, the large acceptance coverage of the CLAS, and the use of tagged photoinduced reactions using the Tagger spectrometer. The reaction $\gamma d \to K^+\Lambda n$ gives indirect access to the Yn interaction through FSI between the hyperon and the spectator nucleon as depicted in panel (d) of Fig. 6. According to the available theoretical models [16; 17], several additional

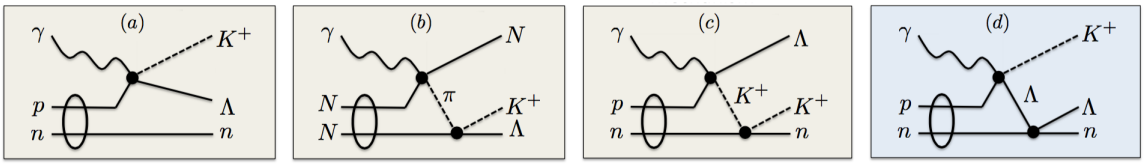

Fig. 6 Four main mechanisms that contribute to the reaction $\gamma d \to K^+\Lambda n$ according to theoretical models []: (a) quasi-free Λ photoproduction on the proton; (b) pion mediated production; (c) K^+ rescattering on spectator neutron; (d) Λ rescattering on spectator neutron.

mechanisms contribute to the reaction of interest, including the pion mediated reaction (panel b), kaon rescattering (panel c), and the quasi-free hyperon photoproduction (panel a). The exclusivity of the reaction allows us to select kinematics that minimise contributions from the quasi-free mechanism, which dominates the cross section. This capability enhances contributions from FSI (panels b-d), permitting the extraction of information on the dynamics of the YN interaction in a model-dependent way. The most comprehensive model currently available provides calculations for the unpolarised cross section, as well as single and double polarisation observables [16; 18]. The model predictions are based on two YN potentials (Nijmegen NSC89 and NSC97f), both of which correctly predict the hypertrition

binding energy [19]. The model prediction clearly indicate the need of polarisation observables as these are more sensitive to the underlying dynamics and allow a cleaner extraction of information. A large sample of polarisation observables will place stringent constraints on the theoretical models and allow us to extract information of the dynamics of the YN interaction.

Experiment E06-103 [12] utilised both linearly and circularly polarised photon beams giving access to 8 observables (see Eq. (1))

$$\frac{d\sigma}{d\Omega} = \left(\frac{d\sigma}{d\Omega}\right)_0 [1 - P_{lin}\Sigma\cos 2\phi + \alpha\cos\theta_x(-P_{lin}O_x\sin 2\phi - P_{circ}C_x) \\ -\alpha\cos\theta_y(-P_y + P_{lin}T\cos 2\phi) - \alpha\cos\theta_z(P_{lin}O_z\sin 2\phi + P_{circ}Cz)]\,, \quad (1)$$

where $\left(\frac{d\sigma}{d\Omega}\right)_0$ is the unpolarised cross section, P_{lin} and P_{circ} are the degree of linear and circular polarisation, respectively, and Σ, O_x, O_z, C_x, C_z, P_y, and T are the polarisation observables. The kaon azimuthal angle ϕ, and the direction cosines $\cos\theta_{x,y,z}$ of the Λ decay products are defined in Fig. 7. The self-analysing power of Λ, which allows the determination of the Λ polarisation by studying the distribution of its decay products is denoted by α. The experimental conditions resulted to an

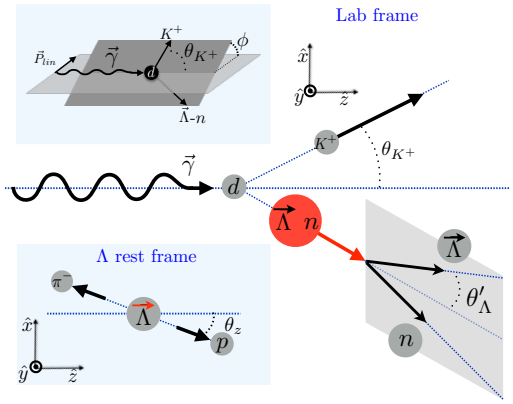

Fig. 7 Reaction plane definition for $\gamma d \to K^+\Lambda n$. The upper left panel defines the kaon azimuthal angle ϕ, in which Σ produces a modulation (see Eq. (1). The lower left panel shows the definition of θ_z (and correspondingly θ_x) in which the double polarisation observables produce modulations. The kaon polar angle and the hyperon angle θ'_Λ, which polarisation observables are predicted to be sensitive to are defined in the main figure.

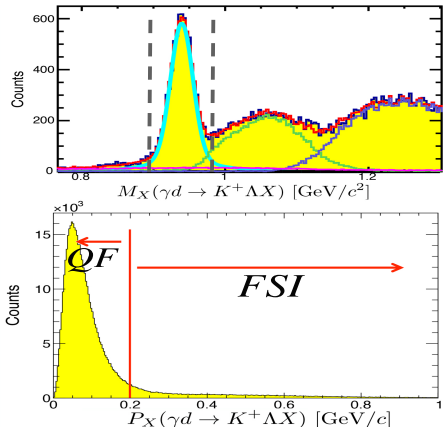

Fig. 8 Top panel: Missing-mass distribution of the reaction $\gamma d \to K^+\Lambda X$ fitted with contributions from $\gamma d \to K^+\Sigma^0 X$ (green), $\gamma d \to K^+\Sigma^* X$ (purple), and accidental events (magenta) from simulated data. The vertical dotted lines indicate the cuts that select the events of interest and the fits are used to perform background subtraction. Bottom panel: Missing momentum of the reaction $\gamma d \to K^+\Lambda X$ indicating the cut applied to select FSI.

average photon polarisation of 75% for the linearly polarised data and between 30% and 80% for the circularly polarised data. The analysis of these data included the selection of three-charged track events identified as one proton, one kaon, and one pion. Hyperon events were selected from studying the $p-\pi^-$ invariant mass, and the reaction was reconstructed from the missing-mass technique of $\gamma d \to K^+\Lambda X$. The upper panel of Fig. 8 shows this missing-mass distribution, where a clear neutron peak can be seen lying on top of a smooth background from Σ^0 and Σ^* photoproduction events. Contributions from these background channels were extensively studied utilising a comprehensive event generator and a realistic detector simulation and subtracted from our total yield.

The exclusivity of the reaction allowed us to reconstruct the momentum of the missing neutron and select events in which FSI dominate. This was done by analysing events in which the neutron had momentum higher than the typical Fermi momentum (see lower panel of Fig. 8). Preliminary results for photon energies between 1.0 and 2.4 GeV, kaon momenta between 0.3 and 1.9 GeV/c, and θ'_Λ angles between 0 and 60 degrees were determined using an unbinned maximum likelihood technique that minimised acceptance and method-related systematic uncertainties. The determination of the single polarisation observable Σ using the azimuthal distribution of the hyperon or the neutron (in addition

of the kaon azimuthal distribution) provides us further information on kinematics where specific FSI mechanisms contribute and a way to disentangle these contributions.

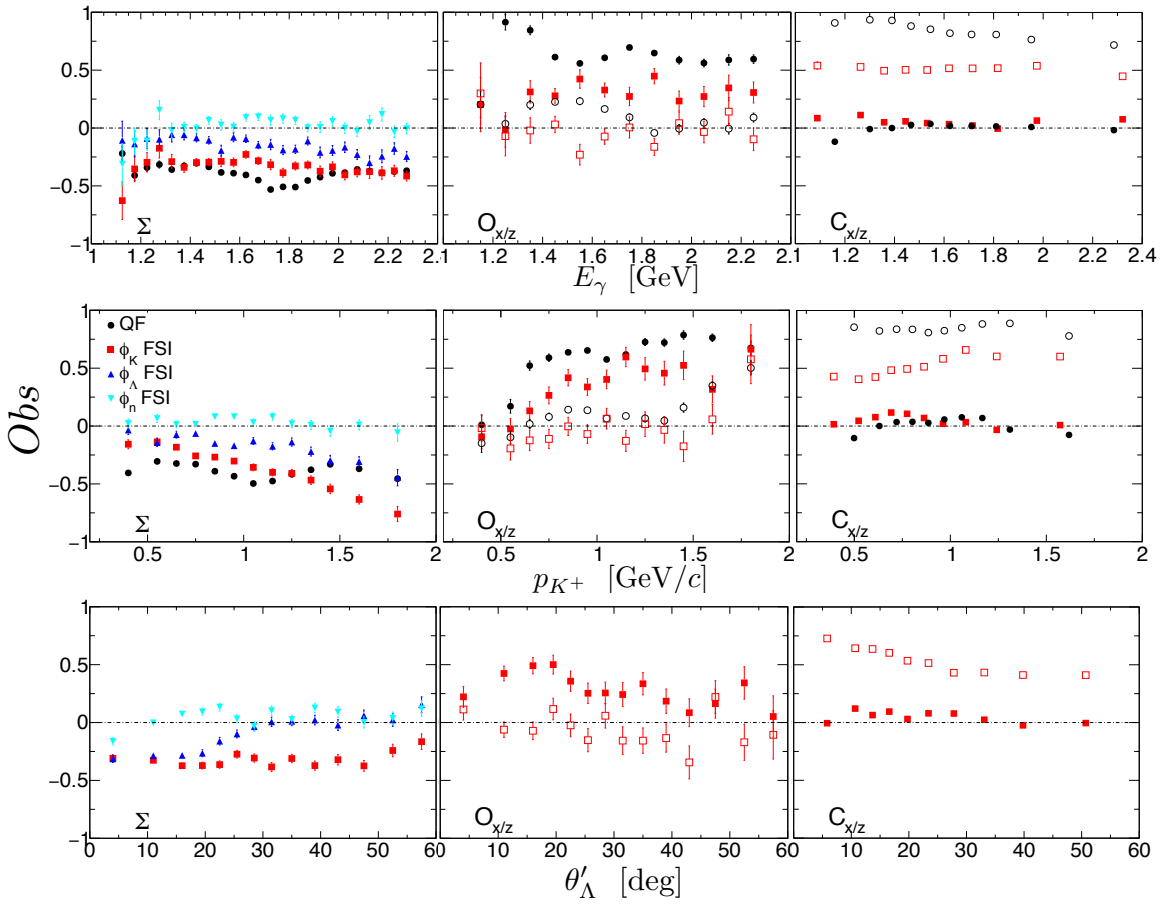

Fig. 9 First preliminary results for the quasi-free (black points) and FSI in the reaction $\gamma d \to K^+\Lambda n$. The FSI results are determined using the kaon azimuthal angle (red markers) for the double polarisation observables. The beam spin-asymmetry is also determined using the hyperon and reconstructed neutron azimuthal distribution (blue and cyan markers, respectively). For the double polarisation observables the solid markers represent the transverse polarisation transfers and the open markers the longitudinal polarisation transfers. The rows show the one-fold differential results for photon energy, kaon momentum, and hyperon angles respectively.

The first preliminary results (see Fig. 9) clearly indicate that the quality of the one-fold (shown) and many-fold differential data allows a detailed study of the kinematical dependence of several observables. This is essential for studying the underlying dynamics in a model-dependent way and we are well underway of using our many-fold differential results to constrain the free parameters of the available models. In addition, the ongoing detailed study of the beam-spin asymmetry determined using the azimuthal distribution of all final-state particles provides us with the information we need to estimate contributions from the various FSI mechanisms. Therefore, a precise determination of the beam-spin asymmetry might allow us to isolate the YN interaction obtaining the first ever information on polarisation observables from this mechanism. Furthermore, a detailed study of the quasi-free reaction ($\gamma p \to K^+\Lambda$) observables from deuterium target will allow us to better understand initial-state effects or even develop tools to extract information from free neutron targets by mapping out the fermi-momentum dependence of polarisation observables. Such methods can be validated by comparing the extrapolated results with the currently available high-statistic data from free proton targets also collected with CLAS [20].

References

1. C.W. Leemann, D.R. Douglas, and G.A. Krafft (2001) The Continuous Electron beam Accelerator Facility: CEBAF at the Jefferson Laboratory. Annu. Rev. Nucl. Part. Sci. 51:413–50
2. B.A. Mecking *et. al.* (2003) The CEBAF large acceptance spectrometer (CLAS). Nucl. Instr. Meth. A 503:513–53
3. S.J. Brodsky and G. Farrar (1973) Scaling laws at large transverse momentum. Phys. Rev. Lett. 31:1153-6
4. J. Polchinski and M.J. Strassler (2002) Hard rescattering and Gauge/String duality . Phys. Rev. Lett. 88:031601-4
5. B.L. Berman, G. Audit, and P. Corvisiero (1993) Photoreactons on ^{3}He. Jefferson Lab Experiment E93-044
6. I. Pomerantz *et. al.* (2013) Hard two-body photodisintegration of ^{3}He . Phys. Rev. Lett. 110:242301-7
7. P. Rossi *et. al.* (2013) Onset of asymptoric scaling in deuteron photodisintegration. Phys. Rev. Lett. 94:012301-5
8. M. Sargsian (2004) Polarisation observables in Hard Rescattering Mechanism of deuteron photodisintegration. Phys. Lett. B 587:41-51
9. V.Y. Grishina *et. al.* (2004) Forward-backward angle asymmetry and polarisation observables in higj-energy deuteron photodisintegration. Eur. Phys. J. A 19:117-123
10. M. Mirazita *et. al.* (2004) Complete anglular distribution of two-body photodisintegration between 0.5 and 3.0 GeV. Phys. Rev. C 70:014005-12
11. R. Avakian *et. al.* (2008) Determination of the azimuthal asymmetry in deuteron photodisintegration by linearly polarised photons at $E_\gamma = 1.1 - 2.3$ GeV. CLAS Approved Analysis, CAA-NP07-01
12. P. Nadel-Turonski *et. al.*, Kaon production on the deuteron using polarized photons. Jefferson Lab PAC30 Proposal PR-06-103 (2006)
13. N. Zacharioui *et. al.*, Determination of the beam-spin asymmetry of deuteron photodisintegration in the energy region $E_\gamma = 1.1 - 2.3$ GeV. Phys. Rev. C 91:055202-16
14. M. Sargsian (2016) Private Communication.
15. D. Lonardoni, A. Lovato, S. Gandolfi, and F. Pederiva (2015) Hyperon Puzzle: Hints from quantum monte carlo calculations. Phys. Rev. Lett. 114:092301-5
16. A. Salam *et al.* (2006), K^0 photoproduction on the deuteron and the extraction of the elementary amplitude. Phys. Rev. C 74:044004-8
17. J. M. Laget (2007), Pentaquark, cusp, and rescattering in single kaon photoproduction off deuterium. Phys. Rev. C 75:014002-7
18. K. Miyagawa *et al.* (2006), Polarization observables in exclusive kaon photoproduction on the deuteron. Phys. Rev. C 74:034002-11
19. K. Miyagawa *et al.* (1998), The hypertriton and its decays. Nucl. Phys. A 639:297c
20. C.A. Patterson *et al.* (2016), Photoproduction of Λ and Σ^0 hyperons using linearly polarized photons. Phys. Rev. C 93:065201-14